

Energy Transfer Between i-Motif DNA Encapsulated Silver Nanoclusters and Fluorescein Amidite Efficiently Visualizes the Redox State of Live Cells

Yadavalli, Hari Chandana; Kim, Yeolhoe; Jung, Il Lae; Park, Sooyeon; Kim, Tae Hwan; Shin, Jin Young; Nagda, Riddhi; Thulstrup, Peter Waaben; Bjerrum, Morten Jannik; Bhang, Yong Joo; Lee, Phil Hyu; Yang, Won Ho; Shah, Pratik; Yang, Seong Wook

Published in:
Small

DOI:
[10.1002/smll.202401629](https://doi.org/10.1002/smll.202401629)

Publication date:
2024

Document Version
Publisher's PDF, also known as Version of record

Citation for published version (APA):
Yadavalli, H. C., Kim, Y., Jung, I. L., Park, S., Kim, T. H., Shin, J. Y., Nagda, R., Thulstrup, P. W., Bjerrum, M. J., Bhang, Y. J., Lee, P. H., Yang, W. H., Shah, P., & Yang, S. W. (2024). Energy Transfer Between i-Motif DNA Encapsulated Silver Nanoclusters and Fluorescein Amidite Efficiently Visualizes the Redox State of Live Cells. *Small*, 20(40), Article 2401629. <https://doi.org/10.1002/smll.202401629>

General rights

Copyright and moral rights for the publications made accessible in the public portal are retained by the authors and/or other copyright owners and it is a condition of accessing publications that users recognise and abide by the legal requirements associated with these rights.

- Users may download and print one copy of any publication from the public portal for the purpose of private study or research.
- You may not further distribute the material or use it for any profit-making activity or commercial gain.
- You may freely distribute the URL identifying the publication in the public portal.

Take down policy

If you believe that this document breaches copyright please contact rucforsk@kb.dk providing details, and we will remove access to the work immediately and investigate your claim.

Energy Transfer Between i-Motif DNA Encapsulated Silver Nanoclusters and Fluorescein Amidite Efficiently Visualizes the Redox State of Live Cells

Hari Chandana Yadavalli, Yeolhoe Kim, Il Lae Jung, Sooyeon Park, Tae-Hwan Kim, Jin Young Shin, Riddhi Nagda, Peter Waaben Thulstrup, Morten Jannik Bjerrum, Yong Joo Bhang, Phil Hyu Lee, Won Ho Yang,* Pratik Shah,* and Seong Wook Yang*

The redox regulation, maintaining a balance between oxidation and reduction in living cells, is vital for cellular homeostasis, intricate signaling networks, and appropriate responses to physiological and environmental cues. Here, a novel redox sensor, based on DNA-encapsulated silver nanoclusters (DNA/AgNCs) and well-defined chemical fluorophores, effectively illustrating cellular redox states in live cells is introduced. Among various i-motif DNAs, the photophysical property of poly-cytosines (C₂₀)-encapsulated AgNCs that sense reactive oxygen species (ROS) is adopted. However, the sensitivity of C₂₀/AgNCs is insufficient for evaluating ROS levels in live cells. To overcome this drawback, the ROS sensing mechanism of C₂₀/AgNCs through gel electrophoresis, mass spectrometry, and small-angle X-ray scattering is primarily defined. Then, by tethering fluorescein amidite (FAM) and Cyanine 5 (Cy5) dyes to each end of the C₂₀/AgNCs sensor, an Energy Transfer (ET) between AgNCs and FAM is achieved, resulting in intensified green fluorescence upon ROS detection. Taken together, the FAM-C₂₀/AgNCs-Cy5 redox sensor enables dynamic visualization of intracellular redox states, yielding insights into oxidative stress-related processes in live cells.

1. Introduction

Deoxyribonucleic acids (DNAs) have emerged as captivating materials for crafting bioinspired nanomachines.^[1] Leveraging the predictable behavior of Watson-Crick base pairing, researchers have forged a wide array of structural and functional DNA-based nanomaterials. These materials find applications in diverse fields such as nanoelectronics,^[2] material science,^[3] photonics,^[4] biosensing,^[5,6] and bioimaging.^[7] One of the functional DNA-based nanomaterials is DNA-encapsulated fluorescent silver nanoclusters (DNA/AgNCs).^[8–10] The compelling photophysical properties of DNA/AgNCs, including a substantial Stokes shift, robust photostability, and tunable fluorescence, have been demonstrated by several applications in biosensing for nucleic acids, proteins, chemicals, acid-base titration, and

H. C. Yadavalli, Y. Kim, S. Park, R. Nagda, W. H. Yang, S. W. Yang
Department of Systems Biology
Institute of Life Science and Biotechnology
Yonsei University
Seoul 03722, Republic of Korea
E-mail: bionicwono@yonsei.ac.kr; yangsw@yonsei.ac.kr
I. L. Jung
Department of Radiation Biology
Environmental Radiation Research Group
Korea Atomic Energy Research Institute
Daejeon 34057, Republic of Korea

T.-H. Kim
Department of Quantum System Engineering
Jeonbuk National University
Jeonju 54896, Republic of Korea
J. Y. Shin, P. H. Lee
Department of Neurology
College of Medicine
Yonsei University
50 Yonsei-ro, Seodaemun-gu, Seoul 03722, Republic of Korea
P. W. Thulstrup, M. J. Bjerrum
Department of Chemistry
University of Copenhagen
Universitetsparken 5, Copenhagen 2100, Denmark

Y. J. Bhang
Xenohelix Research Institute
BT Centre 305, 56 Songdogwahak-ro Yeonsugu, Incheon 21984, Republic of Korea
P. Shah
Department of Science and Environment
Roskilde University
Roskilde 4000, Denmark
E-mail: shah@ruc.dk

The ORCID identification number(s) for the author(s) of this article can be found under <https://doi.org/10.1002/smll.202401629>

© 2024 The Author(s). Small published by Wiley-VCH GmbH. This is an open access article under the terms of the [Creative Commons Attribution-NonCommercial-NoDerivs](https://creativecommons.org/licenses/by/4.0/) License, which permits use and distribution in any medium, provided the original work is properly cited, the use is non-commercial and no modifications or adaptations are made.

DOI: 10.1002/smll.202401629

more.^[8,10–12] Several parameters such as DNA sequence, DNA secondary structure, spatial arrangement of AgNCs, and chemical environments, collectively influence the photophysical traits of DNA/AgNCs.^[13–19] In the case of DNA secondary structures, many studies explored different DNA secondary structures like duplex DNA, hair-pin DNA, G-quadruplex DNA, i-motif DNA, and Hoogsteen triplex DNA, resulting in the development of sensory DNA/AgNCs tailored for a wide range of biomolecules.^[12,20–23] However, despite growing insights into the arrangement of AgNCs within certain DNA structures, achieving precise control over the synthesis of DNA/AgNCs with predictable properties remains a challenge. For instance, while the tunable fluorescence of cytosine-rich DNA/AgNCs has been demonstrated in many studies,^[13,17,24] the addition of extra DNA sequences for biosensing often limits the color palette or eliminates the emission of cytosine-rich DNA/AgNCs.^[11,14,25]

Reactive oxygen species (ROS) are intriguing small molecules within biological systems. While highly toxic in excessive amounts, ROS has a dual nature, functioning as key signaling molecules in both plants and animals, orchestrating responses to diverse biotic and abiotic stimuli. ROS also plays an essential role in developmental processes, actively participating in cellular proliferation and differentiation.^[26] For instance, the influence of ROS on cancer cells is context-dependent, with an appropriate concentration promoting tumorigenesis and aiding cancer cell progression, while an excessive concentration leads to cellular demise.^[27] Cancer cells respond by upregulating their antioxidant systems to maintain ROS at levels conducive to tumor promotion. In the intricate landscape of cancer, redox regulation interfaces with pivotal aspects such as tumor initiation, proliferation, metastasis, programmed cell death, autophagy, metabolic reprogramming, the tumor microenvironment, therapeutic strategies, and the development of therapeutic resistance, all contributing to the intricate processes of cancer development.^[28,29] Given their pivotal role in diseases such as cancer, neurodegenerative disorders, and diabetes, extensive efforts have been devoted to developing fluorescent probes for visualizing ROS levels within cells. Although conventional fluorescent dyes and fluorescent protein-based methods are available for this purpose, they issue some drawbacks such as photobleaching, photodegradation, pH sensitivity, or the requirement for genetic encoding.

Many studies showed that protein or DNA-templated metal-nanoclusters can be applicable for sensing redox changes. For instance, the red fluorescence of multi-stimuli copper nanoclusters was used for the redox sensor. Papain capped Ag/Au nanocluster emits red fluorescence that is quenched by sensing hydrogen peroxide.^[30] The reversible emission change of a poly-cytosine embedded DNA/AgNCs was used to detect hydrogen peroxide, which is a by-product of the reaction of glucose with glucose oxidase.^[31] Moreover, several studies showed that poly-cytosine DNA embedded in different DNA structural contexts such as G-quadruplex, hairpin, or i-motif encapsulates fluorescent AgNCs with different emission colors and photophysical properties in sensing redox changes.^[32] However, none of the studies using poly-cytosine/AgNCs reported the live cell imaging of the redox state to date. In contrast, two studies utilizing hydrogel-embedded AgNCs and bovine serum albumin (BSA) templated AgNCs demonstrated the feasibility of AgNCs for redox sensing

in live cells.^[12] In this study, we found that adjusting contrast and extending exposure time was necessary for effectively monitoring the redox state in live cells using the fluorescence intensity of the ROS-sensory DNA/AgNCs. To address this limitation, we conducted a comprehensive analysis of the impact of DNA sequence, DNA secondary structure, and chemical composition on the red, blue, and green ROS-sensory DNA/AgNCs, utilizing a range of complementary analytical techniques. Subsequently, to enhance the sensitivity of ROS detection, we integrated the strong and stable fluorophores fluorescein amidite (FAM) and Cyanine 5 Cy5 with the ROS-sensory DNA/AgNCs. Through this approach, we achieved yet undefined energy transfer (ET) between FAM and AgNCs, resulting in the emission of highly stable green fluorescence in response to ROS in live cells.

2. Results and Discussion

To develop an effective ROS-sensor for monitoring the redox state in live cells, we primarily explored a variety of DNA/AgNCs using previously reported poly-cytosine sequences.^[33,34] Among them, we selected poly-cytosine DNA groups and two control DNAs. The group consists of 7 poly-cytosine linear DNAs (C_6 , C_{12} , C_{15} , C_{18} , C_{20} , and C_{24}). The two controls are C_3 repeat DNAs inspired by the plant telomere sequences ($[C_3TA_3]^4$) and a hairpin poly-cytosine DNA (Locking- C_{20}), as shown in Table S1 (Supporting Information). Here, poly-cytosine linear DNA refers to a single-stranded DNA with the repetition of only cytosine (C) bases. In the 7 poly-cytosine linear DNAs, the red fluorescence gradually decreased over time with an increased blue fluorescence building up except for C_6 DNA (Figure S1, Supporting Information). Likewise, the red fluorescence was converted into blue fluorescence in the control $[C_3TA_3]^4$ repeat DNA. However, the conversion did not occur in Locking- C_{20} (Figure S2, Supporting Information). From the poly-cytosine DNA templates, we specifically identified C_{20} DNA as a potential sensor candidate. This selection was based on their distinctive strong red, blue, and green fluorescence and the relatively clear emission shift. Notably, the red fluorescence (Ex/Em: 580 nm/650 nm) of C_{20} /AgNCs converted into a blue emission (Ex/Em: 340 nm/470 nm) or a green emission (Ex/Em: 420 nm/530 nm) (Figure S2A–C, Supporting Information). Furthermore, after an additional 72 h incubation of C_{20} /AgNCs, we observed that no red-emitting AgNCs remained (Figure S2A–C, Supporting Information). While $[C_3TA_3]^4$ /AgNCs effectively underwent a conversion of their red fluorescence (Ex/Em: 580 nm/650 nm) to blue fluorescence (Ex/Em: 340 nm/470 nm) and slight green emission (Ex/Em: 420 nm/530 nm), it slightly retained red fluorescence even after a 72 h incubation (Figure S2D–F, Supporting Information). As a non-i-motif structure, we also examined Locking- C_{20} DNA, which features additional sequences that can form a hairpin structure. In this case, the red fluorescence of Locking- C_{20} /AgNCs diminished, and there was a marginal shift toward blue fluorescence over the course of the oxidation process (Figure S2G–I, Supporting Information). Hence, we did not further investigate the $[C_3TA_3]^4$ and Locking- C_{20} due to their inadequacy as a redox sensor.

Hydrogen peroxide (H_2O_2) is a key molecule for cellular homeostasis in most eukaryotes, where the balance between its production, neutralization, and signaling holds significance.^[35] Therefore, we tested whether the red-to-blue shift by time-dependent

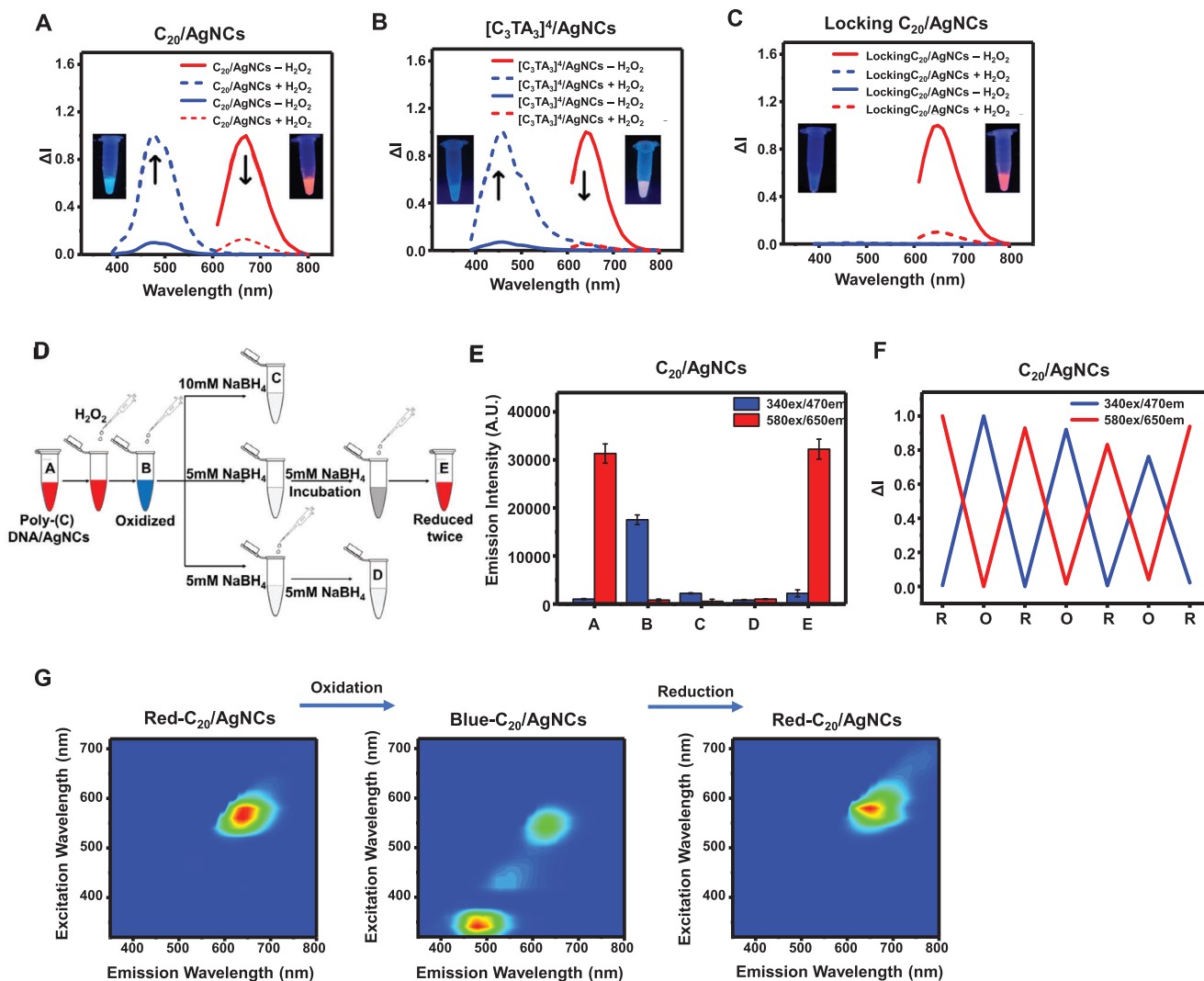


Figure 1. Evolution of red to blue switchable DNA/AgNCs sensors. A–C) Probing the change in standardized fluorescence intensity of $C_{20}/AgNCs$, $[C_3TA_3]^4/AgNCs$, and Locking- $C_{20}/AgNCs$ in the presence and absence of H_2O_2 , respectively. The inset depicts images of DNA/AgNCs visualized under UV illumination (Ex: 365 nm) for before (right) and after (left) adding H_2O_2 , respectively. D,E) Schematic representation D) and comparison E) of the reversibility of Red- $C_{20}/AgNCs$ after oxidation to Blue- $C_{20}/AgNCs$, followed by double reduction with $NaBH_4$. The X-axis in Figure (E) illustrates steps A–E), representing the data obtained from the samples indicated in the schematic representation of Figure (D). F) The relative fluorescence intensity of AgNCs in response to oxidation-reduction changes of C_{20} DNA templates. The samples were incubated for 5 min between each addition of H_2O_2 and $NaBH_4$. O and R represent the oxidized C_{20} DNA/AgNCs, respectively. In reactions A–F) the fluorescence for 340 nm (Blue) and 580 nm (Red) excitation intensities were recorded at the 1 h time point before and after the addition of H_2O_2 respectively. G) Contour plot depicting excitation versus emission for a complete redox cycle of $C_{20}/AgNCs$, respectively. The samples were excited every 10 nm from 320 nm to 720 nm. ΔI represents the emission intensity of DNA/AgNCs normalized to 1. The error bars represent the mean \pm standard deviation (\pm SD) from 3 independent experiments.

oxidation can be expedited by H_2O_2 . Upon adding H_2O_2 , the red fluorescence of all the selected DNA templates rapidly decreased within 1 h; however, the redox-induced blue conversion did not necessarily occur (Figure S3, Supporting Information). For instance, in the first group, $C_6/AgNCs$ did not show any blue conversion (Figure S3A, Supporting Information). $C_{12}/AgNCs$, $C_{15}/AgNCs$, and $C_{20}/AgNCs$ showed faint orange emission (Ex/Em: 480 nm /590 nm) and slight green emission (Ex/Em: 420 nm/530 nm) in addition to the blue conversion (Figure 1A; Figures S3B,C, S4, Supporting Information). Besides, $C_{18}/AgNCs$ showed a clear blue conversion without any additional color emission (Figure S3D, Supporting Information).

$C_{24}/AgNCs$ showed green (Ex/Em: 420 nm/530 nm) and blue emission (Ex/Em: 340 nm/470 nm) without orange emission (Figure S3E, Supporting Information). However, $C_{20}/AgNCs$ displayed strong red fluorescence upon encapsulating AgNCs, and transformed into blue and green fluorescence emitting AgNCs after oxidation (Figure 1A,G; Figure S4, Supporting Information). We further investigated the time-dependent transition between red (Ex/Em: 580 nm/ 650 nm) and blue (Ex/Em: 340 nm/ 470 nm) fluorescence intensities after oxidation. Likewise, $[C_3TA_3]^4/AgNCs$ showed clear blue fluorescence and slight green emission (Figure 1B). The control Locking- $C_{20}/AgNCs$ lost its red fluorescence but did not generate blue fluorescence

(Figure 1C). Upon adding H₂O₂, the red fluorescence of all the selected DNA templates rapidly decreased within 1 h; whereas blue fluorescence increased. The blue fluorescence of the nanoclusters was retained up to 72 h indicating the high stability of the Blue-C₂₀/AgNCs and [C₃TA₃]⁴/AgNCs. However, the Locking-C₂₀/AgNCs lost its red fluorescence without generating blue fluorescence (Figure S5, Supporting Information). Due to the higher intensity of both red and blue (green) fluorescence observed in C₂₀/AgNCs in comparison to the other poly-cytosine linear DNA and [C₃TA₃]⁴/AgNCs, we chose C₂₀/AgNCs for a ROS-sensor. Next, we assessed the sensitivity of C₂₀/AgNCs by decreasing the H₂O₂ concentration *in vitro*. The result indicated the peak blue conversion of C₂₀/AgNCs at 20 mM of H₂O₂. The minimal detectable concentration of H₂O₂ for sensing related to the linear relationship was determined to be 100 nM (Ex/Em: 340 nm/470 nm, A.U. = 4.2 × 10²) (Figure S6A,B, Supporting Information). Moreover, it was observed that variations in pH did not significantly affect the red-to-blue conversion, but the highest blue conversion was at pH levels of 6.5 and 7.0 (Figure S6C–E, Supporting Information). Previous studies reported the repetitive reversibility of oxidation and reduction reactions between red and green emissive AgNCs.^[20,31] Therefore, we tested whether the redox-dependent color conversion between the red and blue states of C₂₀/AgNCs is feasible. We noted that the converting of blue into red requires a distinct two-stepwise addition of the reducing agent (NaBH₄). This observation potentially indicated the presence of a dark intermediate state of AgNCs consistent with the previous report.^[20] The first addition of NaBH₄ (5 mM) converted the blue AgNCs encapsulated in C₂₀ DNA into dark AgNCs. Subsequently, the second addition of NaBH₄ (5 mM) resulted in the complete regeneration of the red AgNCs which stands out compared to the previous report (Figure 1D,E).^[20] When an equivalent amount of NaBH₄ was added in a single step or consecutively without a brief incubation, the blue AgNCs turned into dark AgNCs without regeneration of red AgNCs (Figure 1E). The serial red-to-blue and blue-to-red conversions were repeated multiple times without altering the intensity and patterns of both blue and red emissions (Figure 1F,G). These results suggested that the red-to-blue (green) conversion through redox changes establishes C₂₀/AgNCs as a feasible redox sensor. Despite the rapid production rate of H₂O₂ in tumor cells, the endogenous concentration is maintained at the range of 10–50 μM, which far exceeds that of normal cells.^[36,37] Therefore, we considered that the C₂₀/AgNCs can be utilized to monitor cancer-mediated or stress-induced bursts of H₂O₂, rather than homeostatic changes in H₂O₂ levels in normal cells. Hence, we explored the potential of C₂₀/AgNCs as a ROS-sensor *in vivo*. First, we introduced Red-C₂₀/AgNCs (Reduced) and Blue-C₂₀/AgNCs (Oxidized) separately into HCT-116 cells, well-studied colon cancer cells, monitoring fluorescence at 470 nm and 650 nm after 12 h using a confocal microscope (Figure 2). While Blue-C₂₀/AgNCs remained unchanged, a small portion of Red-C₂₀/AgNCs was oxidized, converting to Blue-C₂₀/AgNCs within the incubation period, due to the basal ROS in the cells (Figure 2). This result mirrored the characteristics of C₂₀/AgNCs sensor observed *in-vitro*, where the conversion of Red-C₂₀/AgNCs to Blue-C₂₀/AgNCs immediately occurs upon exposure to ROS. In contrast, the reverse conversion necessitates a two-step treatment, indicating the stability of Blue-C₂₀/AgNCs *in vivo*. To verify that the color conver-

sion is induced by ROS in the cell, we treated HCT-116 cells with Sodium Arsenite (NaAsO₂), a known endoplasmic reticulum (ER) stress inducer that rapidly elevates cellular ROS levels, in the presence of either Red-C₂₀/AgNCs or Blue-C₂₀/AgNCs.^[38,39] Indeed, we observed significantly increased conversion from Red-C₂₀/AgNCs to Blue-C₂₀/AgNCs after 12 h (Figure 2). We verified the functionality of the C₂₀/AgNCs redox sensor via three additional biological repeats (Figure S7, Supporting Information). To further validate the feasibility of C₂₀/AgNCs as a ROS sensor in other cell types and to rule out the possibility that the shift in red-to-blue emission of C₂₀/AgNCs is caused by NaAsO₂, we monitored the ROS changes in SH-SY5Y cells, a thrice-subcloned cell line derived from neuroblastoma cell lines.^[40] In the controls, we observed the red fluorescence from Red-C₂₀/AgNCs with faint Blue-C₂₀/AgNCs fluorescence. The faint Blue-C₂₀/AgNCs fluorescence observed in the controls may represent the basal level of ROS for cellular homeostasis. However, upon the treatment of triacylglycerol (TG), a known cellular ROS inducer, in the form of a lipid emulsion (1–3 μM), the Red-C₂₀/AgNCs fluorescence was notably converted into Blue-C₂₀/AgNCs fluorescence in a concentration-dependent manner (Figure S8, Supporting Information).^[41,42] Taken together, these results clearly indicated that the photophysical convertibility of C₂₀/AgNCs is functional in live cells.

However, the intensity of fluorescence in response to ROS in live cells was insufficient to efficiently monitor the redox state in live cells, without a high contrast adjustment. To improve the intensity of the C₂₀/AgNCs redox sensor, we investigated whether photophysical convertibility by ROS is attributed to conformational changes in the structure or alternations in the size of silver clusters within C₂₀/AgNCs. In the gel electrophoresis analysis, the blue state of C₂₀/AgNCs showed migration at a level consistent with that of the red state of C₂₀/AgNCs (Figure 3A). This result indicated that conformational change in the secondary structure of C₂₀/AgNCs may be insignificant. By performing small angle X-ray scattering (SAXS) analysis, we observed a reduction in the radius of silver clusters within the Red-C₂₀/AgNCs (3.24 ± 0.15 nm) compared to the Blue-C₂₀/AgNCs (2.76 ± 0.14 nm) (Figure 3B). The volume of red and blue (green) AgNCs were ≈147 nm³ and ≈88 nm³, respectively. The 60% reduction in the volume of AgNCs may be attributed to increased compactness or a decrease in the number of silver atoms. Hence, employing electrospray ionization (ESI)-mass spectroscopy, we conducted a comparison of the number of silver atoms in both the Blue- and the Red-C₂₀/AgNCs. The Red-C₂₀/AgNCs exhibited three prominent MS peaks, Ag⁷ (charge –4; m/z 1616.58), Ag¹⁴ (charge –4; m/z 1805.41) and Ag¹⁹ (charge –4; m/z 1993.78), while the Blue-C₂₀/AgNCs showed prominent peaks for Ag⁷ and Ag⁸ (charge –4; m/z 1643.05) (Figure 3C,D). In the ESI-mass spectroscopy, we only detect small amount of AgNCs with less than 8 Ag atoms, upon the sensor was exposed to ROS. The intensity counts of Ag⁷ in the Red-C₂₀/AgNCs were halved in the Blue-C₂₀/AgNCs (Figure 3D), however, C₂₀/AgNCs with Ag⁷ (with 6 or 7 Ag⁺) is presence in both samples indicates that these AgNCs are not attributed to the fluorescent AgNCs. Previously, two studies reported that Ag¹⁴ and Ag¹⁵ exhibited the highest quantum yields for red fluorescence.^[43,44] Based on these studies we ruled out the Ag¹⁹ (with 8 or 9 Ag⁺) to be responsible for the origin of red emission. Furthermore, our result indicated that the red-to-blue

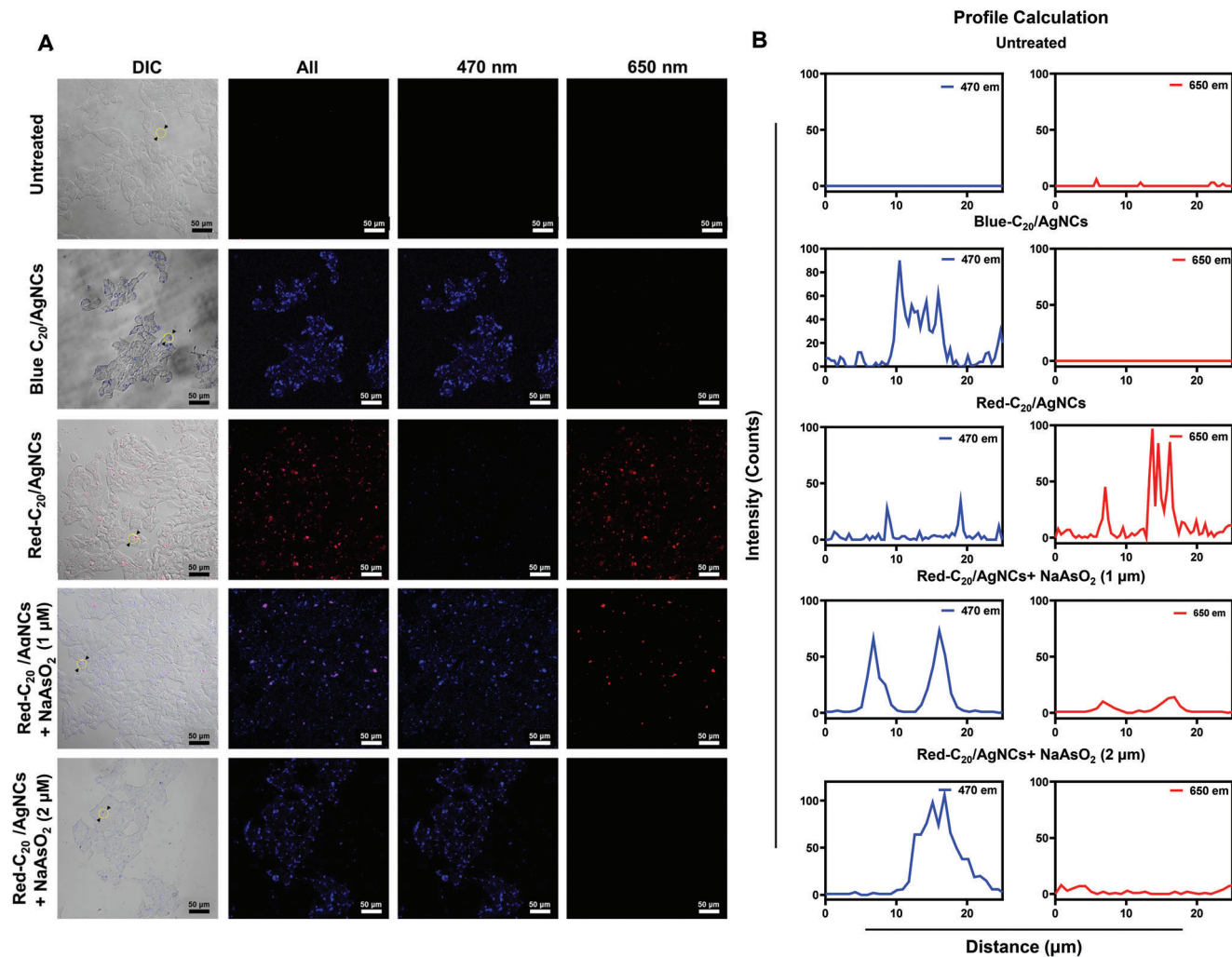


Figure 2. Live cell imaging of ROS using C₂₀/AgNCs sensor. A) HCT-116 cells were observed with confocal microscopy after transfection with Blue- and Red-C₂₀/AgNCs for 12 h. To induce the level of ROS in the cells, two different concentrations of Sodium Arsenite (1 and 2 μM) were treated in the transfected cells with Blue- and Red-C₂₀/AgNCs. All images were taken using a 20X objective with a scale bar of 50 μm. The data were analyzed with three biological replicates (*n* = 3). B) The emission intensity profiles for both blue (left) and red (right) fluorescence calculated for the cells at the 20X magnification images in each set. To avoid bias, all cells were treated with lipofectamine.

conversion has a correlation between the disappearance of the Ag¹⁴ peak and the emergence of the Ag⁸ peak. Thus, we speculated that the blue and red emission comes from Ag⁸ (with 8 Ag⁺) and Ag¹⁴ (with 6 or 7 Ag⁺), respectively (Figure 3C,D). These results were consistent to the 60% reduction in the volume of Blue-C₂₀/AgNCs compared to Red-C₂₀/AgNCs with the SAXS data (Figure 3B). We assumed that variations in the distribution of Ag⁺/Ag⁰ or differences in the structural arrangements of Ag between blue and green AgNCs could potentially modify the photo-physical properties, despite the involvement of the same number of Ag atoms. Cytosine-rich sequences often give rise to quadruplex DNA structures involving Cytosine–Cytosine base pairing, known as i-motif DNA structures.^[45] This structure has previously been demonstrated to encapsulate redox-responsive fluorescent AgNCs on multiple occasions.^[21,46] Hence, we explored the potential involvement of the i-motif structure in the conversion of red and blue AgNCs. Using circular dichroism (CD)

spectroscopy, we analyzed the red and blue states of C₂₀/AgNCs. The characteristic CD signature, featuring negative and positive peaks at ≈265 nm and ≈285 nm, respectively, is exhibited by i-motif DNA structures.^[45,46] We observed the formation of the i-motif structure in both the non-clustered C₂₀ DNA control and the Red-C₂₀/AgNCs, displaying a positive peak at ≈282 nm and a negative peak at ≈263 nm (Figure 3E,F). In contrast, upon oxidation, both the structural confirmation of C₂₀ DNA and the Blue-C₂₀/AgNCs underwent significant changes, showing no positive peak but only a negative peak at ≈270 nm. The DNA conformation was restored completely when the Blue-C₂₀/AgNCs were reduced to the Red-C₂₀/AgNCs (Figure 3F). The reversible conversion between two conformations of DNA/AgNCs can be observed through multiple cycles of oxidation/reduction (Figure S9A, Supporting Information). Using UV/Vis spectrophotometry, we observed the absorbance of Red-C₂₀/AgNCs at 374 nm, 443 nm, and 540 nm (Figure 3G). We speculated that the

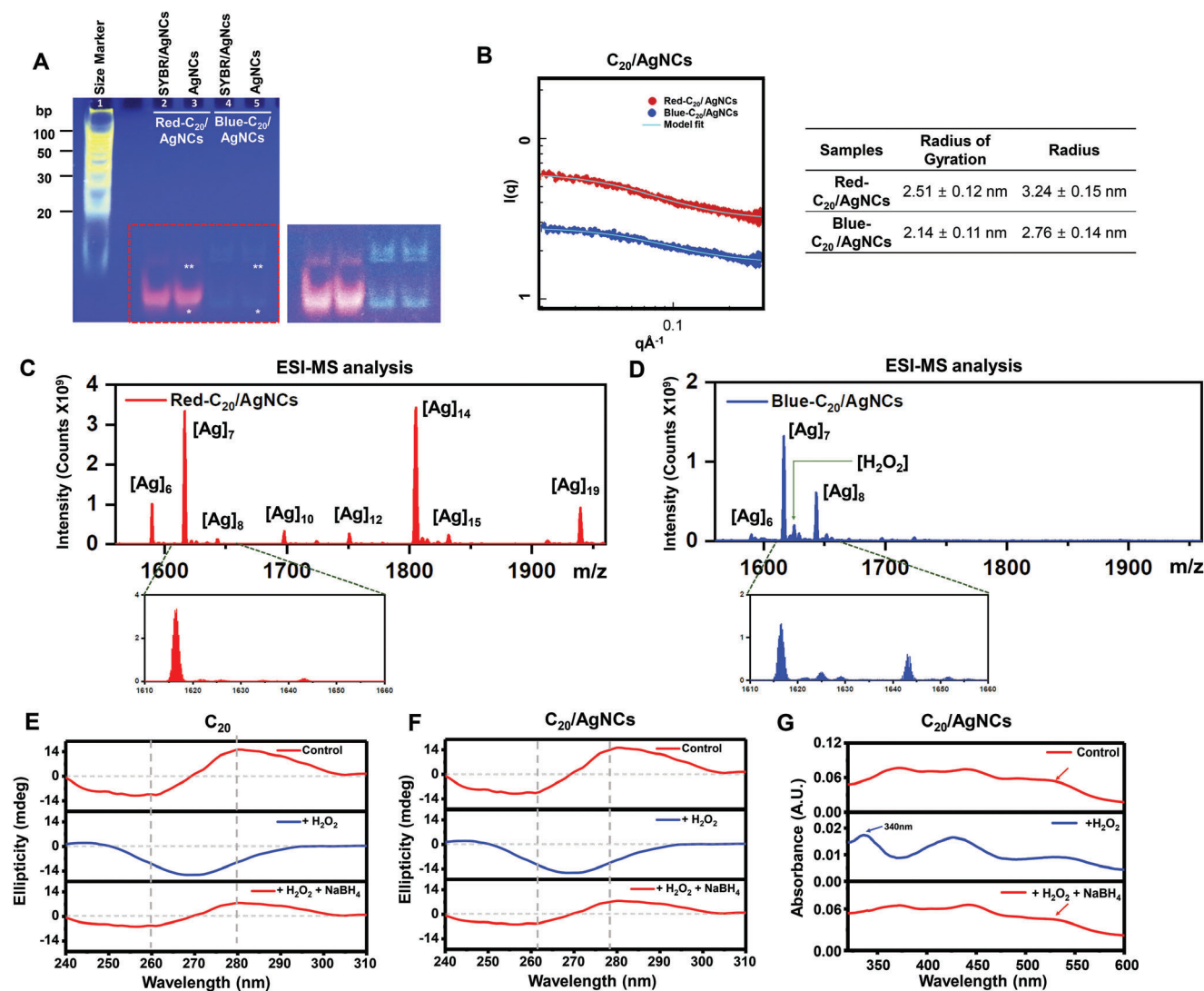


Figure 3. Correlations among fluorescent shift, absorbance, cluster size, and the numbers of silver atoms within $C_{20}/AgNCs$ during the oxidation and reduction process. A) In-gel fluorescence assay of Red- and Blue- $C_{20}/AgNCs$. The blue band corresponds to the oxidation of Red- $C_{20}/AgNCs$ prior to gel electrophoresis. Samples in all lanes except 2 and 4 were treated with SYBR Gold (SYBR) DNA staining solution. The intensified region highlighted in red features single and double asterisks, illustrating the structures encapsulating both red- and blue- fluorescent AgNCs. B) SAXS analysis of $C_{20}/AgNCs$ before and after oxidation along with a table depicting their respective size measurements. C, D) ESI-Mass spectroscopy shows the number of silver atoms in Red- $C_{20}/AgNCs$ and Blue- $C_{20}/AgNCs$. E, F) CD spectroscopy of C_{20} DNA and $C_{20}/AgNCs$ during oxidation and subsequent reduction processes. G) UV absorption spectra of $C_{20}/AgNCs$ during redox changes.

absorption peak at 540 nm corresponds to the Red- $C_{20}/AgNCs$, while the 443 nm absorbance is likely associated with minor green AgNCs species. However, upon oxidation, the absorbance at 540 nm decreased notably, and a new absorption peak emerged at 339 nm (Figure 3G). This observation aligned with the reduced fluorescence of Red- $C_{20}/AgNCs$ and the appearance of Blue- $C_{20}/AgNCs$ with an excitation wavelength of 340 nm. Upon reducing the Blue- $C_{20}/AgNCs$ with a reductant, the absorbance peak at 374 nm, 443 nm, and 540 nm reappeared (Figure 3G). We confirmed that the absorbance conversion between red and blue AgNCs can be repeated over multiple cycles (Figure S9B, Supporting Information). Notably, the alteration of the i-motif structure in C_{20} DNA upon oxidation was distinguishable from pH-induced alterations (Figure S9C, Supporting Information).

These results clearly demonstrated the correlation between the DNA secondary structure and the red-to-blue (green) conversion upon oxidation. For instance, in reduced conditions, the i-motif structure of C_{20} DNA encapsulates red emissive AgNCs. However, upon oxidation, the alteration of the i-motif structure in C_{20} DNA prevents the embedding of Ag,¹⁴ resulting in the generation of blue emissive AgNCs. In summary, we posit that the conformational change in the i-motif structure of C_{20} DNA appears to be a prerequisite to the emission conversion of $C_{20}/AgNCs$ in response to redox changes. Based on these findings, we speculated that the emission intensity of $C_{20}/AgNCs$ may be difficult to sensitize solely through simple template sequence substitution, nucleic acid modification, or adjustments to the properties of AgNCs without the incorporation of additional fluorophores.

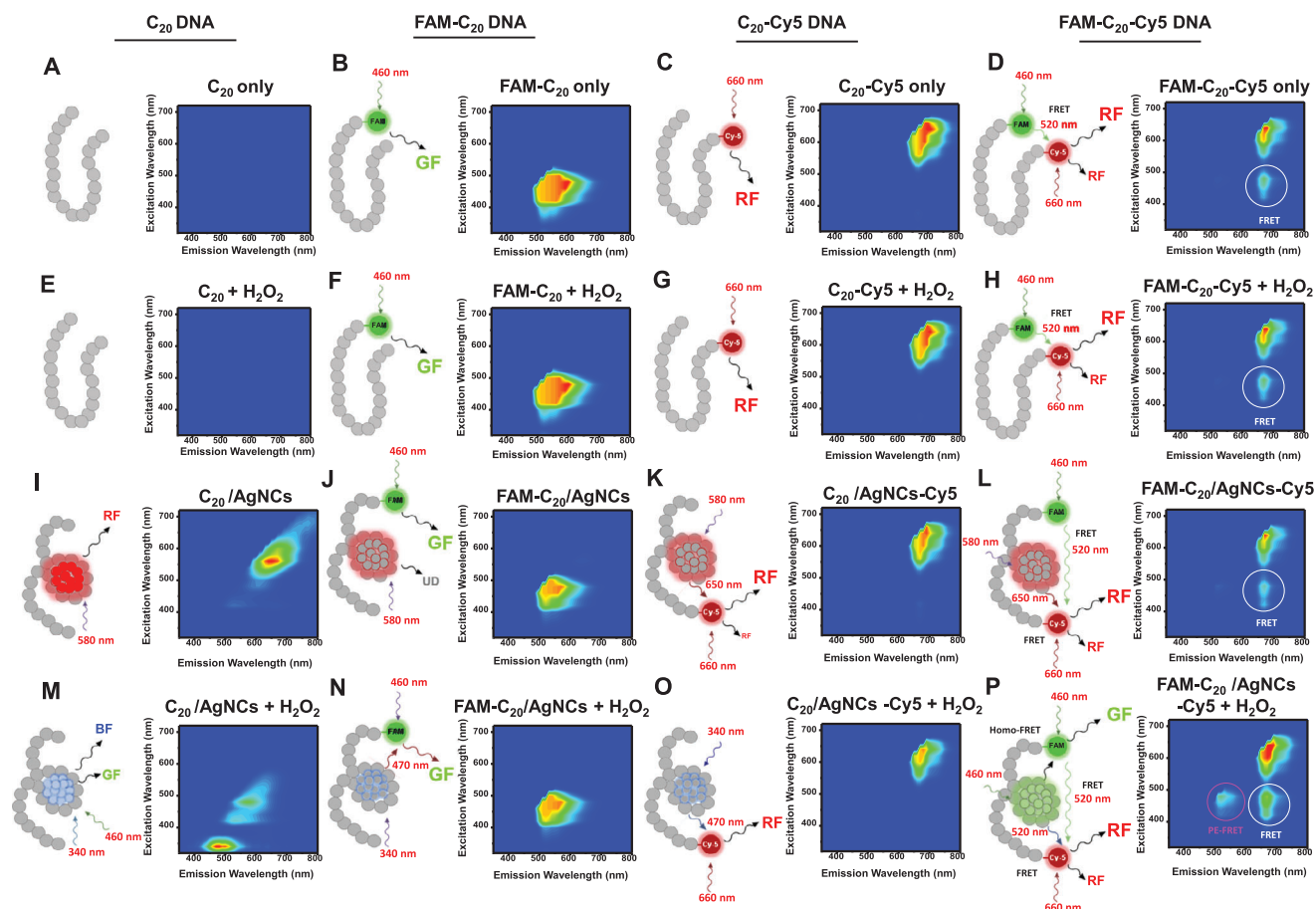


Figure 4. Development of ROS sensing system based on homogenous FRET or NSET using FAM-C₂₀/AgNCs-Cy5 sensor. A–D) The excitation/emission profiles of C₂₀, FAM-C₂₀, C₂₀-Cy5, and FAM-C₂₀-Cy5 DNA only, E–H) in the presence of H₂O₂, (I–L) after the formation of DNA/AgNCs and M–P) after the DNA/AgNCs were treated with H₂O₂. All schematics of the predicted structures have been shown on the left of their respective figures to indicate the excitation profiles and the energy transfers between the molecules. BF, GF, and RF indicate blue fluorescence, green fluorescence, and red fluorescence, respectively. The white and pink circles denote homogenous FRET or NSET, respectively. The downward arrows represent the excitation profile of the sample observed. The samples were excited and monitored every 10 nm from 320 nm to 720 nm.

It has been widely accepted that the photoluminescence (PL) quenching of molecular fluorophores by non-emissive gold nanoparticle (AuNP) acceptors is not solely attributed to a classical Fluorescence Resonance Energy Transfer (FRET) process. The potential explanations of the phenomena encompass FRET, Nanosurface Energy Transfer (NSET), and neither of these processes.^[47–50] Recently, several studies reported various forms of energy transfer between chemical fluorophores and gold nanoclusters. For instance, the significant enhancement of AuNCs luminescence rather than the expected quenching of the chemical fluorophores. AuNCs act as FRET donors for dyes and AuNPs.^[51] Likewise, Amaro et. al., showed a possibility of the energy transfer from AgNCs to Yb³⁺ Ions in Co-Doped GeO₂-PbO Glasses.^[52] Hence, we hypothesized that the FRET between two stable fluorophores, FAM and Cy5, can be an adjustable beacon by adopting the photophysical convertibility of AgNCs in the C₂₀ DNA template. First, we separately labeled fluorophores either at the 5' end and 3' end of the C₂₀ DNA template, referred to as FAM-C₂₀ DNA and C₂₀-Cy5 DNA, respectively. We observed the typical green fluorescence from FAM-C₂₀ DNA (Ex/Em: 480 nm/520 nm, A.U. = 2.6 × 10⁷) and deep red fluo-

rescence from C₂₀-Cy5 DNA (Ex/Em: 660 nm/700 nm, A.U. = 4.2 × 10⁷), while the C₂₀ DNA without fluorophores exhibited no fluorescence (Figure 4A–C; Figure S10A, Supporting Information). When the C₂₀ DNA was tethered with both the FAM and Cy5, referred to as FAM-C₂₀-Cy5 DNA, we observed a distinct FRET between FAM as a donor and Cy5 as an acceptor. The green fluorescence of FAM (A.U. = 2.6 × 10⁷) excited at 480 nm was dropped by 70% (A.U. = 1.1 × 10⁷) because the emitted energy of FAM transferred to Cy5, resulting in the emission of deep red fluorescence (Ex/Em: 480 nm/700 nm, A.U. = 6.4 × 10⁶). The deep red fluorescence from C₂₀-Cy5 DNA (A.U. = 2.4 × 10⁵), when it was excited at 480 nm, was only 4% of that observed with FAM-C₂₀-Cy5 DNA (A.U. = 6.4 × 10⁶), confirming the FRET between FAM and Cy5 (Figure 4D; Figure S10A, Supporting Information). If FAM-C₂₀-Cy5 DNA was directly excited at 660 nm, it also generated deep red fluorescence (A.U. = 2.5 × 10⁷). However, the intensity is 60% of that observed with C₂₀-Cy5 DNA (A.U. = 4.2 × 10⁷). Furthermore, to rule out the possible influence of redox change on FAM and Cy5 dyes, we treated H₂O₂ on the four C₂₀ DNA templates: C₂₀ DNA, FAM-C₂₀ DNA, C₂₀-Cy5 DNA, and FAM-C₂₀-Cy5 DNA without encapsulating AgNCs.

The green and red fluorescence from the C₂₀ DNA tethering the stable chemical dyes remained unaltered, showing the insensitivity of these dyes to ROS. When FAM-C₂₀-Cy5 DNA was excited at 480 nm, it generated deep red emission at 700 nm (A.U. = 2.5 × 10⁷), showing that the FRET between FAM and Cy5 remained unaffected even in the presence of ROS (Figure 4E–H; Figure S10B, Supporting Information). Next, we used the four C₂₀ DNA templates for encapsulating AgNCs. As shown earlier, we observed the red fluorescence from Red-C₂₀/AgNCs (Figure 4I). The green fluorescence of FAM-C₂₀ DNA (A.U. = 2.6 × 10⁷) was unaltered in FAM-C₂₀/AgNCs (A.U. = 2.5 × 10⁷). In the case of C₂₀/AgNCs-Cy5 (Ex/Em: 660 nm/700 nm, A.U. = 4.0 × 10⁷), it showed almost the same level of deep red fluorescence as that of C₂₀ DNA-Cy5 (Ex/Em: 660 nm/700 nm, A.U. = 4.2 × 10⁷) (Figure 4J,K; Figure S10A,C, Supporting Information). These results indicated that no FRET occurs between FAM and Red-C₂₀/AgNCs and between Cy5 and the Red-C₂₀/AgNCs. Next, we investigated the influence of AgNCs on the fluorescence of FAM-C₂₀-Cy5 DNA. FAM-C₂₀/AgNCs-Cy5 showed nearly identical levels of green (Ex/Em: 480 nm/520 nm, A.U. = 1.2 × 10⁷) and deep red fluorescence (Ex/Em: 660 nm/700 nm, A.U. = 2.2 × 10⁷) compared to those of FAM-C₂₀-Cy5 DNA (Figure 4L; Figure S10C, Supporting Information). These results confirmed that Red-C₂₀/AgNCs do not affect the fluorescence of FAM and Cy5, and vice versa. Upon the treatment of H₂O₂ to the AgNCs-embedded C₂₀ DNA templates, the red fluorescence from Red-C₂₀/AgNCs was converted into the blue and green fluorescence from Blue-C₂₀/AgNCs (Figure 4M). Besides, the green fluorescence from FAM-C₂₀/AgNCs remained unaltered when excited at 480 nm (A.U. = 2.7 × 10⁷), and the deep red fluorescence from C₂₀/AgNCs-Cy5 were maintained at 660 nm (A.U. = 4.1 × 10⁷) (Figure 4N,O; Figure S10D, Supporting Information). In the case of FAM-C₂₀/AgNCs-Cy5, upon treatment with H₂O₂ and excited at 480 nm, the quenched FAM emission (A.U. = 1.1 × 10⁷) was dramatically increased by around three folds (A.U. = 3.4 × 10⁷) (Figure 4P; Figure S10D, Supporting Information). Remarkably, the emission intensity of FAM-C₂₀/AgNCs-Cy5 (A.U. = 3.4 × 10⁷) was one thousand times higher than the blue fluorescence of C₂₀/AgNCs (A.U. = 4.1 × 10⁴) in response to H₂O₂ (100 nm) (Figure S10E, Supporting Information). Despite the significantly higher intensity of FAM-C₂₀/AgNCs-Cy5 compared to the C₂₀/AgNCs sensor, the minimal concentration of H₂O₂ for sensing, as determined by the linear relationship, was found to be 100 nm (Figure S10F, Supporting Information). The rationale behind this finding is justified, as the sensing mechanism for H₂O₂ relies on the photochemical properties of the C₂₀/AgNCs sensor. Upon adding H₂O₂, the green fluorescence of FAM-C₂₀/AgNCs increases rapidly by 20 min and stabilized up to 72 h, indicating the high stability of FAM-C₂₀/AgNCs-Cy5 (Figure S10G, Supporting Information). Furthermore, FAM-C₂₀/AgNCs-Cy5 emitted 40% higher deep red fluorescence (Ex/Em: 480 nm/700 nm, A.U. = 9.8 × 10⁶) compared to that of FAM-C₂₀/AgNCs-Cy5 without H₂O₂ (Ex/Em: 480 nm/700 nm, A.U. = 6.3 × 10⁶) (Figure S10C, Supporting Information). Based on these results, we considered a scenario for the mechanism responsible for the intensified green fluorescence and enhancement of deep red fluorescence in FAM-C₂₀/AgNCs-Cy5. Upon the H₂O₂ treatment, C₂₀/AgNCs oxidized to generate green emission (Ex/Em: 480 nm/530 nm) that transfers energy to FAM, possibly through homogenous FRET

(Homo-FRET) or NSET, intensifying the green fluorescence of FAM. This speculation can be evidenced by three factors. First, the green emissions of C₂₀/AgNCs (Ex/Em: 480 nm/520 nm A.U. = 1.1 × 10⁴) were increased three-fold by H₂O₂ treatment (Ex/Em: 480 nm/520 nm A.U. = 3.9 × 10⁴) (Figure S10D, Supporting Information). Second, even though previous studies mainly reported that the energy transfer from chemical dyes to metal nanoclusters,^[53] in our observation, the energy seemed to transfer from FAM to C₂₀/AgNCs was insignificant. For instance, there was no big difference between the emission intensity of FAM-C₂₀ DNA and FAM-C₂₀/AgNCs at 480 nm excitation. Third, the 40% increase in deep red emission of FAM-C₂₀/AgNCs-Cy5 at 480 nm excitation may indicate the occurrence of energy transfer from C₂₀/AgNCs to Cy5 via FAM. This inference is supported by the deep red fluorescence observed at 480 nm excitation in C₂₀/AgNCs-Cy5 with (A.U. = 8.4 × 10⁴) or without H₂O₂ treatment (A.U. = 9.8 × 10⁴), which did not show any direct sign of energy transfer between C₂₀/AgNCs and Cy5 (Figure 4O; Figure S11C–D, Supporting Information). Although the energy transfer from C₂₀/AgNCs to FAM was undefined, we evidently observed that FAM-C₂₀/AgNCs-Cy5 shows three-fold higher green fluorescence than that of FAM-C₂₀-Cy5 DNA, upon treatment of H₂O₂ (Figure S11D, Supporting Information), implying the critical role of AgNCs. Given that the plasmonic enhancement of AgNCs on FRET between two chemical fluorophores in the previous study,^[54] the nanosurface energy transfer between AgNCs and FAM could be one of the potential answers for this phenomenon.

As a next step, we validated whether the FAM-C₂₀/AgNCs-Cy5 can be functional as a redox sensor in live cells, comparing its performance to C₂₀/AgNCs. Under normal conditions for 12 h followed by transfection of Red-C₂₀/AgNCs maintained its red fluorescence, possibly due to its relatively weak sensitivity. Likewise, FAM-C₂₀/AgNCs-Cy5 showed basal green fluorescence (520 nm) from FAM and a relatively higher deep red fluorescence (700 nm) from Cy5. However, we were unable to see the red fluorescence (650 nm) from AgNCs in FAM-C₂₀/AgNCs-Cy5 (Figure 5). Upon induction of internal ROS using Sodium Selenite (1 μM), Red-C₂₀/AgNCs immediately converted into Blue-C₂₀/AgNCs, emitting blue fluorescence, consistent with previous observations (Figure 2). In the case of FAM-C₂₀/AgNCs-Cy5, the redox change in the cells led to a dramatic increase in the green fluorescence from FAM, while the deep red fluorescence was slightly enhanced when excited at 660 nm. However, we were unable to see the blue fluorescence AgNCs in FAM-C₂₀/AgNCs-Cy5 (Figure S10D, Supporting Information). Using FAM-C₂₀/AgNCs and C₂₀-Cy5/AgNCs as controls, we confirmed the ROS-induced intensification of green fluorescence by AgNCs in live cells (Figure S11A, Supporting Information). The intensity of green and deep red fluorescence of FAM-C₂₀/AgNCs and C₂₀-Cy5/AgNCs, respectively, was unaffected by the treatment of Sodium Arsenite (Figure S11B, Supporting Information). Furthermore, we tested the functional property of FAM-C₂₀/AgNCs-Cy5, compared to MitoSOX, a cell-permeable ROS indicator that selectively targets mitochondria. As shown in Figure S12 (Supporting Information), FAM-C₂₀/AgNCs-Cy5 can be comparable to other chemical redox sensors for two reasons: permeability and intensity. We believe that the dual-channel feature of FAM-C₂₀/AgNCs-Cy5 with both green and deep red fluorescence serves two purposes. The green channel indicates at change in

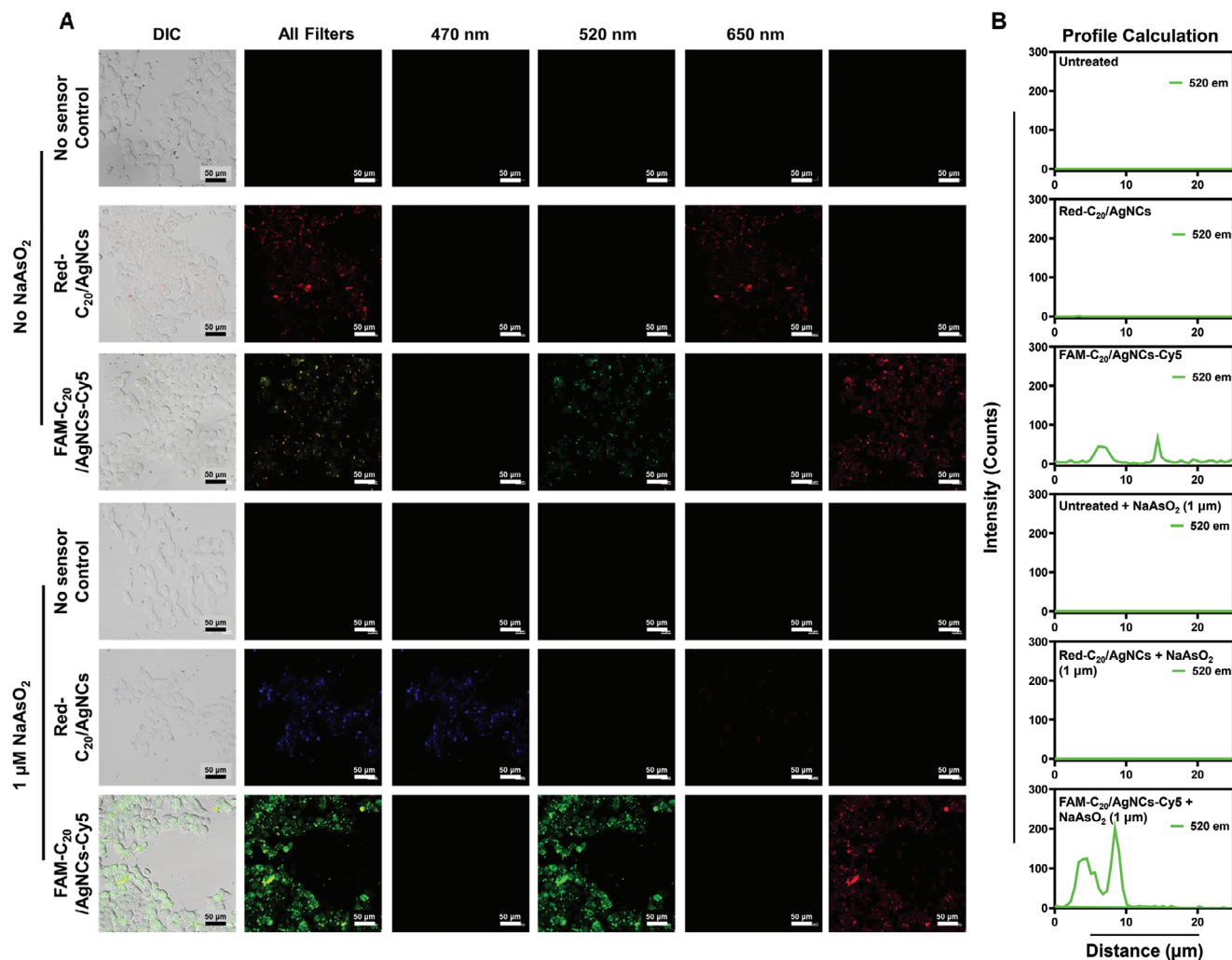


Figure 5. Live cell imaging of ROS using FAM- C_{20} /AgNCs-Cy5 sensor. A) Confocal microscopic images of HCT-116 cells untreated or treated with Red- C_{20} /AgNCs and FAM- C_{20} /AgNCs-Cy5 for 12 h. To induce the level of ROS in the cells, Sodium Arsenite ($1 \mu\text{M}$) was treated in the transfected cells with Red- C_{20} /AgNCs and FAM- C_{20} /AgNCs-Cy5. To avoid bias all the cells were treated with lipofectamine. All images were taken at a 20X magnification with a scale bar of $50 \mu\text{m}$. B) The emission intensity profile green fluorescence by FAM, calculated for a cell, is depicted for the 20X magnification images in each set.

the redox state, while the deep red channel ensures the distribution of the sensor inside cells. This dual-channel capability is expected to be advantageous for comprehensive redox sensing applications.

3. Conclusion

Many studies have employed poly-cytosine encapsulated fluorescent AgNCs for redox sensing. Ritchie *et al.*, utilized C_{12} DNA and reported the blue shift in the emission color of red emissive AgNCs due to oxidation.^[55] Similarly, Choi *et al.*, found that C_{24} DNA-encapsulated nanoclusters exhibit varying responses to different oxidants, generating blue-emissive AgNCs.^[23] Furthermore, Lim *et al.*, recently demonstrated that C_{20} DNA induces the conversion of red emissive AgNCs to blue emissive AgNCs over time.^[22] Despite the efforts made in the aforementioned studies, the detailed mechanism underlying the red-to-blue emis-

sion conversion of poly-cytosine DNA/AgNCs in response to redox changes has remained uncharted. Moreover, practical applications as a redox sensor in live cells have been scarcely explored. In this study, we proposed several important findings through diverse approaches. First, the disruption and reformation of the i-motif of C_{20} DNA are repetitively convertible in response to redox changes, determining the size of embedded AgNCs. Second, the number of silver atoms confined in the i-motif emitting red fluorescence is tentatively 14; if the AgNC is oxidized and the i-motif is disrupted, the confined number of silver atoms reduces to 8, emitting blue and green fluorescence, depending on the excitation wavelength. Third, the red-to-blue (green) conversion of C_{20} /AgNCs is insensitive to a wide range of pH changes (pH: 5 to 10), ensuring that the specificity of C_{20} /AgNCs for redox sensing. When the metallic nanoparticles are illuminated with light, they can support surface plasmons. The presence of surface plasmons can enhance the local

electromagnetic field around the nanoparticles. This enhanced field, in turn, affects the excitation and emission of nearby fluorophores involved in FRET. This phenomenon has potential applications in various fields, including biosensing, imaging, and nanophotonics, where precise control over energy transfer processes is desired.^[56,57] Several studies showed a mechanism that Energy Transfer (ET) acceptor/sensitization properties of gold nanoclusters are attributed to FRET or NSET.^[51] Moreover, a recent study reported that quantum-size silver nanoclusters with delocalized electrons could lead to a possible plasmon coupling.^[58] Here, we demonstrated the feasibility of FAM- C_{20} /AgNCs-Cy5 serving as a redox sensor where FAM and Cy5 dyes are tethered to C_{20} /AgNCs. Under normal conditions, the strong green fluorescence of FAM is quenched by the proximal Cy5, regardless of the red-emissive AgNCs embedded in the C_{20} DNA template. However, in the presence of ROS, the red-emissive C_{20} /AgNCs convert to blue- and green-emissive C_{20} /AgNCs. When it is excited at 480 nm, the green emission from the C_{20} /AgNCs efficiently transfers energy to FAM and Cy5, enhancing the FRET between FAM and Cy5. The enhancement consequently results in the amplification of green fluorescence from FAM, possibly due to an undefined energy transfer mechanism between AgNCs and FAM. Unlike the previous studies, a new finding is that the energy transfer occurs from AgNCs to FAM and Cy5. Remarkably, this mechanism remains functional inside cells. Hence, we propose that the combinatorial integrations of various DNA templates, colorful AgNCs, and well-studied chemical fluorophores may pave the way for new advancements in biosensing and cellular imaging. Furthermore, we believe that a detailed photophysical analysis of the undefined energy transfer mechanism will be the next challenge.

4. Experimental Section

Oligonucleotides and Chemicals: All oligos were obtained from mBiotech, (IDT company, Korea) or Bioneer Co., Ltd., Korea. Oligos were dissolved in DEPC water to obtain a stock concentration of 100 μM . FAM and Cy5 labeled oligonucleotides were purified using HPLC before receiving. Silver Nitrate (AgNO_3 , >99.99%), Sodium Borohydride (NaBH_4 , 99.99%), and Sodium Arsenite ($\text{NaAsO}_2 \geq 90\%$) were purchased from Sigma-Aldrich. Hydrogen peroxide (H_2O_2 , 30% w/v) was obtained from FUJIFILM Wako Pure Chemical Corporation. 40% Acrylamide: Bis-acrylamide (19:1) was purchased from Sigma Aldrich (Yongin City, Korea), TEMED (tetramethylethylenediamine) from Bio-Rad (Hong Kong, China).

Synthesis of DNA/AgNCs: For the synthesis of fluorescent AgNCs, a reaction mixture of 25 μL containing 15 μM of DNA oligo, was denatured at 95 $^\circ\text{C}$ for 10 min and annealed at 25 $^\circ\text{C}$ for 20 min. Then AgNO_3 and NaBH_4 were added and vortexed each to a final concentration of 250 μM in a reaction mixture of 50 μL . These samples were prepared systematically to obtain optimal results. The concentration of nucleic acid here is given for a total reaction volume of 50 μL . The DNA/AgNCs were incubated for 1 h at 25 $^\circ\text{C}$ and eventually used for further analysis. The excitation and emission spectra were measured after dilution to 200 μL using DEPC water. All fluorescent measurements were carried in a 96-well disposable plate using CLARIOstar from BMG Labtech.

Time-dependent & Chemical Oxidation Studies: Samples were prepared as mentioned above for both time-dependent and chemical oxidation studies. For time-dependent oxidation studies, fluorescence of samples was measured at 1, 12, 24, 48, and 72 h time points (after AgNCs were synthesized). Later, for oxidation studies, 20 mM H_2O_2 (30% w/v) was added to the fluorescent DNA/AgNCs, and the fluorescence for 340 nm and 580 nm excitation intensities were recorded at the 1 h time point. In all reactions,

15 μM of DNA oligo, 250 μM AgNO_3 , and NaBH_4 , in a final volume of 50 μL were used. All fluorescent measurements were carried in a 96-well disposable plate using CLARIOstar from BMG Labtech.

Reaction Kinetics of the DNA/AgNCs in the Presence of H_2O_2 : A reaction mixture of 25 μL containing 15 μM of DNA oligo, was denatured at 95 $^\circ\text{C}$ for 10 min and annealed at 25 $^\circ\text{C}$ for 20 min. Then AgNO_3 and NaBH_4 were added and vortexed each to a final concentration of 250 μM in a reaction mixture of 50 μL . 20 mM H_2O_2 (30% w/v) was added to the fluorescent DNA/AgNCs, and the fluorescence for 340 nm and 580 nm excitation intensities were recorded at the 1, 12, 24, 48, and 72 h time points (after oxidation). The excitation and emission spectra were measured after dilution to 200 μL using DEPC water. Origin-2017 software was utilized for fitting exponential models to experimental data of various time points. All fluorescent measurements were carried in a 96-well disposable plate using CLARIOstar from BMG Labtech.

pH Optimization of C_{20} /AgNC Sensor: Samples were prepared as mentioned above for pH and concentration optimization studies. For pH-dependent oxidation studies, fluorescence of samples was measured at various pH ranging from 5 to 10 (using Tris Acetate buffer). Later, for oxidation studies, 20 mM H_2O_2 (30% w/v) was added to the fluorescent DNA/AgNCs, and the fluorescence for 340 nm and 580 nm excitation intensities were recorded at the 1 h time point. In all reactions, 15 μM of DNA oligo, 250 μM AgNO_3 , and NaBH_4 , in a final volume of 50 μL were used. All fluorescent measurements were carried in a 96-well disposable plate using CLARIOstar from BMG Labtech.

Determining Concentration Limit of H_2O_2 for DNA/AgNC Sensor: When testing the minimum and maximum concentration limit, varying concentrations of (0, 0.1, 0.5, 1, 5, 25, 50, 100 μM) and (5, 10, 20, 40, 80 mM) H_2O_2 (30% w/v) were added to Red- C_{20} /AgNCs and the fluorescence for 340 nm and 580 nm excitation intensities were recorded at the 1 h time point. For fluorescence emission spectra measurements, DEPC water was added (final volume 200 μL) to all DNA/AgNCs samples and transferred to a 96-well disposable plate for fluorescence measurements. Origin-2017 software was utilized for fitting linear models to experimental data of various concentration points. All fluorescent measurements were carried in a 96-well disposable plate using CLARIOstar from BMG Labtech.

Reduction of C_{20} Templated DNA/AgNCs: A sample at each oxidation state was prepared with an overall control. The reduction was achieved by adding different amounts of NaBH_4 (5, 10, and [5+5] mM) at different time intervals and for each step to the respective samples in a final volume of 55 μL . Every set of samples was incubated at room temperature for different time periods at 10, 5, and 10 min respectively. Samples were checked frequently to analyze reduction. In all reactions, 15 μM of DNA oligo, 250 μM AgNO_3 , and NaBH_4 , in a final volume of 50 μL were used. All fluorescent measurements were carried in a 96-well disposable plate using CLARIOstar from BMG Labtech.

Oxidation-Reduction Studies: A sample at each oxidation point was prepared using their respective control. Oxidation-reduction cycling was done once the first set of Red-DNA/AgNCs, and Blue-DNA/AgNCs with the highest Ex/Em were prepared as controls. Oxidation-reduction was achieved by adding 20 mM H_2O_2 (30% w/v) and 10 mM of NaBH_4 for each cycle. The concentrations mentioned here were for a final volume of 200 μL . The samples were incubated for 5 min between each addition of H_2O_2 or NaBH_4 . In all reactions, we used 15 μM of DNA oligo, 250 μM AgNO_3 , and NaBH_4 , in a final volume of 50 μL . All fluorescent measurements were carried in a 96-well disposable plate using CLARIOstar from BMG Labtech.

CD Spectroscopy: Four samples of 50 μL each were prepared as mentioned above and combined to a final volume of 200 μL with the DNA concentration of 15 μM . 20 mM H_2O_2 , 10 mM of NaBH_4 were used for oxidation and reduction respectively. JASCO J-815 spectropolarimeter equipped with a CDF-426S Peltier Type CD/fluorescence cell holder maintained at 25 $^\circ\text{C}$ was used to obtain the circular dichroism spectra. Quartz Hellma (105250QS) cuvettes were used to measure the samples.

SAXS Analysis: The final concentration of the samples synthesized for DNA-AgNCs was scaled up to 1 mg mL^{-1} of DNA. DNA probes (200 μL) were denatured at 95 $^\circ\text{C}$ for 10 min, followed by annealing at 25 $^\circ\text{C}$ for 20 min. Equimolar concentrations of 250 μM AgNO_3 and NaBH_4 were

added to a final reaction volume of 200 μL . 20 mM H_2O_2 was used to convert red DNA/AgNCs to blue DNA/AgNCs. The reaction mixtures were incubated at room temperature for an hour. For SAXS analysis, the samples were prepared as described above and were transferred into a standard quartz X-ray capillary tube with a diameter of 1.0 mm. The SAXS measurements were conducted on a microfocussed rotating anode-type laboratory source with a monochromatic (Cu-K α radiation) X-ray beam (Rigaku, NANOPIX model). The sample-to-detector distance was 40 cm, which covered the q range of $0.015 < q, \text{\AA}^{-1} < 0.45$. The background intensity was subtracted from the sample intensity. Silver behenate (AgBe) was used to calibrate the q range.

ESI-MS Analysis: DNA-encapsulated silver nanoclusters underwent analysis via Electrospray Ionization Mass Spectrometry (ESI-MS) in the negative mode utilizing a Solarix XR Bruker mass spectrometer with a lower and upper event limits between 150 m/z and 4000 m/z . DNA silver nanoclusters were prepared as described and used without additional purification. Samples ranging from 5 μL to 25 μL from the preparation were immediately before the measurement diluted with 300–600 μL of 5 mM ammonium formate (pH 7) and then injected directly into the Solarix XR Bruker mass spectrometer at a flow rate of 420 $\mu\text{L h}^{-1}$. The MS was operated at a drying gas temperature of 200 $^\circ\text{C}$ at 4 L min^{-1} along with a capillary voltage of 3400 V. Operating parameters included an in-source collision energy of 60 V. Data acquisition involved 16 to 64 scans within a collection window typically spanning 400 to 800 $m z^{-1}$ around the signals of interest. Data collection and subsequent analysis were conducted using Compass fms control and the Compass data analysis software. In all reactions, 15 μM of DNA oligo, 250 μM AgNO_3 , and NaBH_4 , in a final volume of 50 μL were used. 20 mM H_2O_2 was used to convert red DNA/AgNCs to blue DNA/AgNCs.

In-Gel Fluorescence Assay: For the detection of i-motif and random coil structures of the as-synthesized DNA/AgNCs were analyzed using native polyacrylamide gel electrophoresis (PAGE) (12%) in a MiniPROTEAN Tetra Cell system (Bio-Rad) with TBE buffer (Tris base (44.5 mM), Boric acid (44.5 mM), EDTA (1 mM)). DNA/AgNCs were prepared as depicted above. To half of the 50 μL reaction mixture, with 2.25 μL of 50% glycerol and 0.5 μL of 200X SYBR Red dye (SYBR Gold Nucleic Acid Gel Stain, Thermo Fisher Scientific S11494) were added. NATIVE PAGE was performed at 90 V/1 h followed by visualization under the UV transilluminator. A Canon EOS 750D DSLR camera with an EF-S 18–55 mm lens was used to capture the gel images under UV light. In all reactions, 15 μM of DNA oligo, 250 μM AgNO_3 , and NaBH_4 , in a final volume of 50 μL were used. 20 mM H_2O_2 was used to convert red DNA/AgNCs to blue DNA/AgNCs.

ROS Sensing System Based on Homogenous FRET or NSET Using Fluorescent Tagged C_{20} DNA: For determining homogenous FRET or NSET using FAM or Cy-5 tagged C_{20} /AgNCs, the samples were prepared as mentioned above. 250 μM of AgNO_3 and NaBH_4 were not added to DNA only but were compensated with DEPC water. Additionally, Oxidation was performed using 20 mM H_2O_2 . The excitation and emission spectra were measured at the 1 h time point after dilution to 200 μL using DEPC water. All fluorescent measurements were carried in a 96-well disposable plate using CLARIOstar from BMG Labtech.

Cell Culture: The human colorectal carcinoma cell line (HCT-116, SH-SY5Y) was purchased from the American Type Culture Collection (ATCC, Gangnam-gu, Korea). All cell lines were cultured in DMEM high glucose medium with 1% penicillin-streptomycin and 10% Fetal bovine serum (FBS) in a humidified CO_2 incubator under sterile conditions. DMEM media used for cell culture was purchased from Welgene (Gyeongsangsi, Korea). HCT-116 colon cancer cells were cultured in DMEM (Dulbecco's Modified Eagle Medium) supplemented with 10% FBS (fetal bovine serum). The cell lines were maintained in a humidified atmosphere containing 5% CO_2 at 37 $^\circ\text{C}$. The cells were seeded at 2×10^5 cells in 2 mL of growth media (1×10^5 cells mL^{-1}) and grow it to optimal density for transfection. Cell culture media used was Welgene's DMEM high glucose, 10% Gibco's fetal bovine serum, and 1% penicillin-streptomycin.

Live Cell Imaging of ROS Using Redox Sensor DNA/AgNC Probes: In a well with 2 mL culture media of a 6-well plate, 135 μL of Opti-MEM media were cultured for 24 h. A transfection reagent with a final volume of (10 μL)

lipofectamine and 300 nm of Red- and Blue- C_{20} /AgNCs was first prepared or FAM- C_{20} -AgNCs-Cy5 and incubated at RT for 5 min. Then the cells were incubated with transfection reagent for 12 h. The cells were incubated with and without respective concentrations of NaAsO_2 and incubated at RT for 1 h. The cells were washed three times with 1X PBS prior to imaging. To avoid bias, all cells including controls were treated with lipofectamine. It was the same method of treatment for all cells, except that DNA/AgNCs were not added to the untreated cells. All cell culture experiments were performed thrice ($n = 3$ biological replicates) with consistent results every time. The microscope used for confocal imaging was Carl Zeiss Confocal laser scanning microscope-880. Zen Blue (V 3.4) software was used to obtain the Merged images and their intensity profiles.

Live Cell Imaging of Triacylglycerol-Induced ROS Using C_{20} /AgNCs Sensor: The cells were cultured and transfected with Red- C_{20} /AgNCs as mentioned above. The cells were incubated with 3 different concentrations of Triacylglycerol. Culture medium and Hanks' Balanced Salt Solution (HBSS) were used as negative controls. The cells were washed three times with 1X PBS prior to imaging. To avoid bias, all cells including controls were treated with lipofectamine. All cell culture experiments were performed thrice ($n = 3$ biological replicates) with consistent results every time. The microscope used for confocal imaging was Carl Zeiss Confocal laser scanning microscope-880. Zen Blue (V 3.4) software was used to obtain the Merged images and their intensity profiles.

Mito-Tracking Dye and FAM- C_{20} -Cy5/AgNCs for Enhanced Redox Sensing: The cells were cultured and transfected with Red- C_{20} /AgNCs as mentioned above. HCT-116 cells were treated with FAM- C_{20} -Cy5/AgNCs at RT for 12 h. The cells were incubated with MitoSOX red (1 h) dye in the absence and presence of 1 μM Sodium Arsenite. The cells were washed three times with 1X PBS prior to imaging. To avoid bias, all cells including controls were treated with lipofectamine. All cell culture experiments were performed thrice ($n = 3$ biological replicates) with consistent results every time. The microscope used for confocal imaging was Carl Zeiss Confocal laser scanning microscope-880. Zen Blue (V 3.4) software was used to obtain the Merged images and their intensity profiles.

Examination of Fluorescence Across Multiple Channels: Blue fluorescence by Blue- C_{20} /AgNCs, detected using the DAPI channel with excitation at 405 nm, with an emission range of 440–480 nm; green fluorescence by FAM, observed using the AF 488 channel with excitation at 488 nm, with an emission range 490–540 nm; red fluorescence by Red- C_{20} /AgNCs, detected using the AF 594 channel with excitation at 561 nm, with an emission range 630–670 nm; and far-red fluorescence by Cy5, observed using the Cy5 channel with excitation at 650 nm, with an emission range 670–720 nm range. The fluorescence emitted by MitoSOX red was observed by a custom filter with excitation at 396 nm, with an emission range 580–630 nm.

Statistical Analyses: Statistical analyses and Figures were generated using Origin 2017 software. The quantitative data analysis was made based on three independent experiments representing mean + standard deviation (SD). In each figure, specific tests and their statistical significance are indicated. A total of three biological repeats ($n = 3$) were conducted in two independent experiments for cell imaging.

Supporting Information

Supporting Information is available from the Wiley Online Library or from the author.

Acknowledgements

This work was supported by the Korea Medical Device Development Fund (KMDF) (RS-2022-00141618), the Korea Health Technology R&D Project through the Korea Health Industry Development Institute (KHIDI), funded by the Ministry of Health & Welfare, Republic of Korea (HU21C0053), the Basic Science Research Program through the National Research Foundation (NRF) (NRF-2018R1A6A1A03025607, 2018R1D1A1B07051125, 2021R1A6A3A13044758, 2022R1F1A1073998, 2022R1A2C10915076, and

2023R1A2C3004112). This research was also supported in part by the Brain Korea 21 (BK21) FOUR (Fostering Outstanding Universities for Research) program from the Ministry of Education (MOE, Korea). H.C.Y. is a recipient of a fellowship awarded by the BK21 FOUR program.

Conflict of Interest

A provisional patent application has been filed based on this work where HCY, SWY, PS and WHY are listed as inventors. YJB is associated with Xenohelix Research Institute which develops new technologies for molecular detection.

Author Contributions

H.C.Y., Y.K., and I.L.J. contributed equally to this work. S.W.Y., P.S., and W. H.Y. conceived the project and wrote the manuscript. R.N., S.P., I.L.J., H.C.Y., Y.K., J.Y.S. performed most of the analyses. H.C.Y., Y.K., W.H.Y., and J.Y.S., conducted cellular imaging. M.J.B, P.W.T. conducted ESI-MS analyses, T.K. performed SAXS analyses. Y.J.B., P.H.L. consulted the project and manuscript.

Data Availability Statement

The data that support the findings of this study are available from the corresponding author upon reasonable request.

Keywords

DNA, energy transfer, imaging, redox sensing, silver nanoclusters

Received: March 1, 2024

Revised: April 21, 2024

Published online:

- [1] N. C. Seeman, H. F. Sleiman, *Nat. Rev. Mater.* **2017**, *3*, 17068.
- [2] L. Hui, R. Bai, H. Liu, *Adv. Funct. Mater.* **2022**, *32*, 2112331.
- [3] Y. Hu, C. M. Niemeyer, *Adv. Mater.* **2019**, *31*, 1806294.
- [4] K. E. Dunn, A. Elfick, *Bioconjugate Chem.* **2023**, *34*, 97.
- [5] U. Singh, V. Morya, A. Rajwar, A. R. Chandrasekaran, B. Datta, C. Ghoroi, D. Bhatia, *ACS Omega* **2020**, *5*, 30767.
- [6] P. D. Howes, S. Rana, M. M. Stevens, *Chem. Soc. Rev.* **2014**, *43*, 3835.
- [7] H. C. Yadavalli, S. Park, Y. Kim, R. Nagda, T.-H. Kim, M. K. Han, I. L. Jung, Y. J. Bhang, W. H. Yang, L. T. Dalgaard, S. W. Yang, P. Shah, *Small* **2023**, *20*, 2306793.
- [8] J. Sharma, H.-C. Yeh, H. Yoo, J. H. Werner, J. S. Martinez, *Chem. Commun.* **2011**, *47*, 2294.
- [9] J. T. Petty, J. Zheng, N. V. Hud, R. M. Dickson, *J. Am. Chem. Soc.* **2004**, *126*, 5207.
- [10] Y.-A. Kuo, C. Jung, Y.-A. Chen, H.-C. Kuo, O. S. Zhao, T. D. Nguyen, J. R. Rybarski, S. Hong, Y.-I. Chen, D. C. Wylie, J. A. Hawkins, J. N. Walker, S. W. J. Shields, J. S. Brodbelt, J. T. Petty, I. J. Finkelstein, H.-C. Yeh, *Adv. Mater.* **2022**, *34*, 2204957.
- [11] P. Shah, P. W. Thulstrup, S. K. Cho, Y.-J. Bhang, J. C. Ahn, S. W. Choi, M. J. Bjerrum, S. W. Yang, *Analyst* **2014**, *139*, 2158.
- [12] J. Li, J. Yu, Y. Huang, H. Zhao, L. Tian, *ACS Appl Mater Interfaces* **2018**, *10*, 26075.
- [13] P. Mastracco, A. González-Rosell, J. Evans, P. Bogdanov, S. M. Copp, *ACS Nano* **2022**, *16*, 16322.
- [14] P. Shah, R. Nagda, I. L. Jung, Y. J. Bhang, S.-W. Jeon, C. S. Lee, C. Do, K. Nam, Y. M. Kim, S. Park, Y. H. Roh, P. W. Thulstrup, M. J. Bjerrum, T.-H. Kim, S. W. Yang, *ACS Nano* **2020**, *14*, 8697.
- [15] D. J. E. Huard, A. Demissie, D. Kim, D. Lewis, R. M. Dickson, J. T. Petty, R. L. Lieberman, *J. Am. Chem. Soc.* **2019**, *141*, 11465.
- [16] D. Schultz, E. G. Gwinn, *Chem. Commun.* **2012**, *48*, 5748.
- [17] C. I. Richards, S. Choi, J.-C. Hsiang, Y. Antoku, T. Vosch, A. Bongiorno, Y.-L. Tzeng, R. M. Dickson, *J. Am. Chem. Soc.* **2008**, *130*, 5038.
- [18] M. Gambucci, C. Cerretani, L. Latterini, T. Vosch, *Methods Appl Fluoresc* **2019**, *8*, 014005.
- [19] J. Sharma, R. C. Rocha, M. L. Phipps, H.-C. Yeh, K. A. Balatsky, D. M. Vu, A. P. Shreve, J. H. Werner, J. S. Martinez, *Nanoscale* **2012**, *4*, 4107.
- [20] C. Cerretani, T. Vosch, *ACS Omega* **2019**, *4*, 7895.
- [21] B. Sengupta, K. Springer, J. G. Buckman, S. P. Story, O. H. Abe, Z. W. Hasan, Z. D. Prudowsky, S. E. Rudisill, N. N. Degtyareva, J. T. Petty, *J Phys Chem* **2009**, *113*, 19518.
- [22] J. Y. C. Lim, Y. Yu, G. Jin, K. Li, Y. Lu, J. Xie, Y. N. Tan, *Nanoscale Adv* **2020**, *2*, 3921.
- [23] S. Choi, S. Park, K. Lee, J. Yu, *Chem. Commun.* **2013**, *49*, 10908.
- [24] E. G. Gwinn, P. O'Neill, A. J. Guerrero, D. Bouwmeester, D. K. Fygenson, *Adv. Mater.* **2008**, *20*, 279.
- [25] R. Nagda, S. Park, I. L. Jung, K. Nam, H. C. Yadavalli, Y. M. Kim, K. Yang, J. Kang, P. W. Thulstrup, M. J. Bjerrum, M. Cho, T.-H. Kim, Y. H. Roh, P. Shah, S. W. Yang, *ACS Nano* **2022**, *16*, 13211.
- [26] J. Checa, J. M. Aran, *J Inflamm Res* **2020**, *13*, 1057.
- [27] J. Wang, D. Sun, L. Huang, S. Wang, Y. Jin, *Oxidative Med. Cell. Longev.* **2021**, *2021*, 8532940.
- [28] J. D. Hayes, A. T. Dinkova-Kostova, K. D. Tew, *Cancer Cell* **2020**, *38*, 167.
- [29] N. F. E. D. O. R. O. F. F., *Ann. Bot.* **2006**, *98*, 289.
- [30] M. Wang, M. Wang, G. Wang, X. Su, *Analyst* **2020**, *145*, 1001.
- [31] A. K. Gupta, A. V. Krasnoslobodtsev, *Nanomaterials* **2023**, *13*, 1299.
- [32] J. Sharma, H.-C. Yeh, H. Yoo, J. H. Werner, J. S. Martinez, *Chem. Commun.* **2010**, *46*, 3280.
- [33] L. E. Yourston, A. Y. Lushnikov, O. A. Shevchenko, K. A. Afonin, A. V. Krasnoslobodtsev, *Nanomaterials* **2019**, *9*, 613.
- [34] S. Park, S. Choi, J. Yu, *Nanoscale Res. Lett.* **2014**, *9*, 129.
- [35] N. Di Marzo, E. Chisci, R. Giovannoni, *Cells* **2018**, *7*, 156.
- [36] Z. Chu, J. Yang, W. Zheng, J. Sun, W. Wang, H. Qian, *Coord. Chem. Rev.* **2023**, *481*, 215049.
- [37] C. M. Doskey, V. Buranasudja, B. A. Wagner, J. G. Wilkes, J. Du, J. J. Cullen, G. R. Buettner, *Redox Biol.* **2016**, *10*, 274.
- [38] R. Ruiz-Ramos, L. Lopez-Carrillo, A. D. Rios-Perez, A. De Vizcaya-Ruiz, M. E. Cebrian, *Mutat. Res. – Genet. Toxicol. Environ. Mutagen.* **2009**, *674*, 109.
- [39] O. Cantoni, E. Zito, A. Guidarelli, M. Fiorani, P. Ghezzi, *Antioxidants* **2022**, *11*, 1034.
- [40] J. Kovalevich, D. Langford, In *Neuronal Cell Culture: Methods and Protocols*, (Eds: S. Amini, M. K. White), Humana Press, Totowa, NJ, **2013**, pp. 9–21.
- [41] A. Castoldi, L. B. Monteiro, N. van Teijlingen Bakker, D. E. Sanin, N. Rana, M. Corrado, A. M. Cameron, F. Hässler, M. Matsushita, G. Caputa, R. I. Klein Geltink, J. Büscher, J. Edwards-Hicks, E. L. Pearce, E. J. Pearce, *Nat. Commun.* **2020**, *11*, 4107.
- [42] E. Aflaki, B. Radović, P. G. Chandak, D. Kolb, T. Eisenberg, J. Ring, I. Fertschai, A. Uellen, H. Wolinski, S.-D. Kohlwein, R. Zechner, S. Levak-Frank, W. Sattler, W. F. Graier, R. Malli, F. Madeo, D. Kratky, *J. Biol. Chem.* **2011**, *286*, 7418.
- [43] D. Schultz, K. Gardner, S. S. R. Oemrawsingh, N. Markešević, K. Olsson, M. Debord, D. Bouwmeester, E. Gwinn, *Adv. Mater.* **2013**, *25*, 2797.
- [44] S. M. Copp, D. E. Schultz, S. Swasey, E. G. Gwinn, *ACS Nano* **2015**, *9*, 2303.
- [45] H. Abou Assi, M. Garavís, C. González, M. J. Damha, *Nucleic Acids Res.* **2018**, *46*, 8038.
- [46] T. Li, N. He, J. Wang, S. Li, Y. Deng, Z. Wang, *RSC Adv.* **2016**, *6*, 22839.
- [47] A. Samanta, Y. Zhou, S. Zou, H. Yan, Y. Liu, *Nano Lett.* **2014**, *14*, 5052.

- [48] B. Nikoobakht, C. Burda, M. Braun, M. Hun, M. A. El-Sayed, *Photochem. Photobiol.* **2002**, 75, 591.
- [49] D. K. Maiti, S. Roy, A. Baral, A. Banerjee, *J Mater Chem* **2014**, 2, 6574.
- [50] J.-M. Liu, J.-T. Chen, X.-P. Yan, *Anal. Chem.* **2013**, 85, 3238.
- [51] E. Oh, A. L. Huston, A. Shabaev, A. Efros, M. Currie, K. Susumu, K. Bussmann, R. Goswami, F. K. Fatemi, I. L. Medintz, *Sci. Rep.* **2016**, 6, 35538.
- [52] A. A. Amaro, G. R. d. S. Mattos, M. V. d. M. Nishimura, J. Dipold, N. U. Wetter, L. R. P. Kassab, *Nanomaterials* **2023**, 13, 1177.
- [53] K. Pyo, M. F. Matus, E. Hulkko, P. Myllyperkiö, S. Malola, T. Kumpulainen, H. Häkkinen, M. Pettersson, *J. Am. Chem. Soc.* **2023**, 145, 14697.
- [54] T. Zhao, T. Li, Y. Liu, *Nanoscale* **2017**, 9, 9841.
- [55] C. M. Ritchie, K. R. Johnsen, J. R. Kiser, Y. Antoku, R. M. Dickson, J. T. Petty, *J Phys Chem* **2007**, 111, 175.
- [56] M. Imani, N. Mohajeri, M. Rastegar, N. Zarghami, *Anal. Biochem.* **2021**, 630, 114323.
- [57] J. Shi, F. Tian, J. Lyu, M. Yang, *J. Mat. Chem. B.* **2015**, 3, 6989.
- [58] Q. Wu, C. Liu, C. Cui, L. Li, L. Yang, Y. Liu, H. Safari Yazd, S. Xu, X. Li, Z. Chen, W. Tan, *J. Am. Chem. Soc.* **2021**, 143, 14573.